Long run-out mechanisms of a landslide triggered by the Mid Niigata Prefecture Earthquake in 2004

Yasuhiko Okada
Hirotaka Ochiai
Ushio Kurokawa
Department of Soil and Water Conservation, Forestry and Forest Products Research Institute,
Tsukuba, Ibaraki, Japan

Keywords: landslide, long run-out mechanisms, pore-pressure, apparent friction angle, fluidisation

ABSTRACT

On October 23 2004, a series of earthquakes hit the mid-region of Niigata Prefecture Japan. These earthquakes triggered more than 1000 landslides of various types with in the regional geological structure of the Tertiary slopes. At a typical fluidised landslide, the light-weight cone-penetrometer tests as well as soil samplings were conducted to examine the long run-out mechanisms. The results of simplified cone-penetration tests revealed that the silt layers thinly sandwiched in the sands increased Nc_{10}-values, which exceeded 50 at about 4 m depth at some points. The stress-controlled dynamic ring shear test under the undrained conditions on sand sample generated a significant build-up of pore-pressure which could explain the fluidised motion of the landslide. A digital terrain model was produced by using the 10-m mesh data of laser profiles after the landslide. In order to examine an effective method for the prediction of future landslide motion by distinct element method, the position around which the main body of landslide slipped away was judged in the terrain model, then the ball elements were produced there. The granular mass flow was simulated, reproducing well the travel distance and deposition of the landslide, in which the interparticle friction angle of numerical ball elements was set at the apparent friction angle obtained from the undrained ring shear test.

1 INTRODUCTION

A series of earthquakes (the main shock is named the Mid Niigata Prefecture Earthquake in 2004, with a magnitude of 6.8) (Japan Meteorological Agency 2004) hit the mid-region of Niigata Prefecture, the north-west part of Japan, on 23 October 2004. It claimed 40 lives and injured about 3000 people. More than 1000 landslides of different types (falls, slides, flows, etc.) were triggered in the regional geological structure consisting of the Tertiary sandy siltstone and thin-bedded alternations of sandstone and mudstone. The damaged Higashiyama Hill region has been well known locally as one of the most landslide prone zones, in which NNE-SSW trending folds prevail. The rainfall intensity was more than 100 mm/day accompanied by the typhoon no. 23 fell in the region three days prior to the earthquakes. Accordingly, the subsurface profile contained much subsurface water before the shaking, increasing the pore-pressure during the shakings and this would certainly have exacerbated the landslide downslope movement.

Figure 1: The view of the Haguro landslide

Figure 2: Subsurface water path

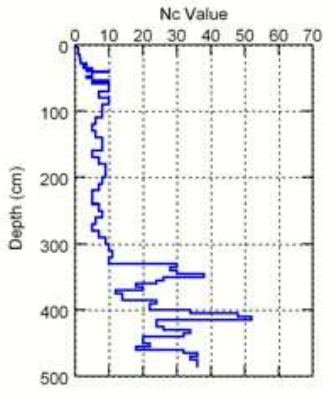

Figure 3: Result of light-weight cone-penetrometer test

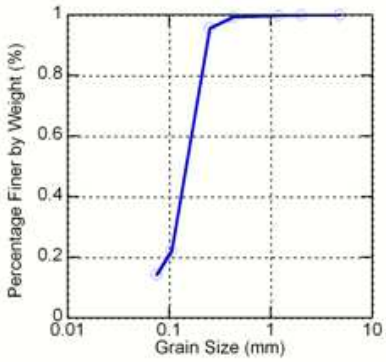

Figure 4: Grain size distribution curve

A typical fluidised landslide occurred in the mostly severely damaged Yamakoshi village (Nagaoka city from April 2005), which travelled on the prefectural road 19 and blocked the Haguro tunnel. The light-weight cone-penetrometer tests [Noguchi et al. 1997] and soil samplings for the permeability investigation and the geotechnical soil tests were exclusively conducted and analysed to explain the fluidised long run-out mechanisms. In order to examine an effective tool for the future landslide motion, the numerical simulation by distinct element method was conducted, in which the digital terrain model was produced by using the 10-m mesh data of laser profiler after the landslide.

2 LANDSLIDE DESCRIPTION

The Haguro landslide took place on a north-facing slope (dip angle was about 35 degrees before landslide occurred), about 12 m deep at the maximum, about 50 m wide, and about 70 m long in the main body. The travel distance was about 280 m and the travel angle was about 21 degrees. The main body deposited on the prefectural road 19 just below the slope and blocked the Haguro tunnel on the right hand bank. Some parts of the debris further flowed down on the left hand bank (Figure 1). The slope mainly consisted of sands, and thin siltstone layers dipping into the slope were observed sporadically. Within the zone of depletion of the landslide, a wet zone about 20 m down from the head-scarp was observed on the 29 November 2004 (more than one month after the landslide). When the place was excavated about 0.3 m by a hand shovel, subsurface water flushed out (Figure 2). Although, after the landslide disaster it did not have such severe rain as that on 23 October, the soils located at around the top of hill slope could contain much subsurface water through subsurface water path, suggesting that when the earthquakes hit, a significant amount of subsurface water was provided by the preceding typhoon no. 23 and contained in the slope.

The light-weight cone-penetrometer tests revealed that the Nc_{10} values increased when encountered the thinly sandwiched siltstone layers, and it, at some points, exceeded 50 at about 4 m deep (Figure 3). The Nc_{10} values are the numbers of times it took to drop a weight (5 kg) from height of 50 cm to drive the cone 10 cm into soils. The sands had the permeability of $k = 4.7\times10^{-5}$ m/s (permeability tests on undisturbed sands specimen were conducted on the samples taken from the source area by 100 ml steep tubes (height = 50 mm)), a specific gravity of Gs = 2.63, a mean diameter of D_{50} = 0.147 mm. The grain size distribution curve is shown in Figure 4.

3 CYCLIC LOADING RING SHEAR TEST UNDER UNDRAINED CONDITIONS

As mentioned above, a large portion of the slope could have contained much subsurface water provided by the typhoon no. 23 during the earthquakes shaking. In order to investigate the fluidised long run-out motion of the landslide, undrained ring shear test were carried out on the disturbed samples taken from the source area, with the aim of examining the pore-pressure behaviours.

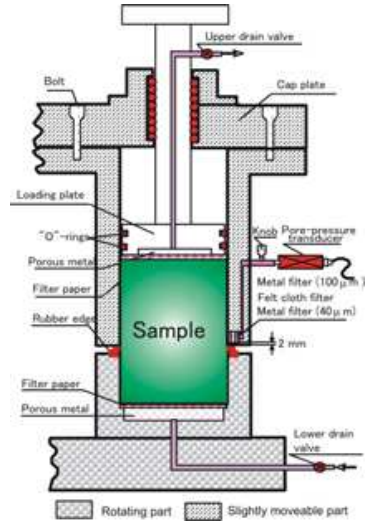

Figure 5: Section through the undrained ring shear box showing the pore pressure measurement

3.1 Testing apparatus

The ring shear test apparatus used is the fifth version of a group of ring shear test apparatuses developed at the Disaster Prevention Research Institute, Kyoto University, Japan. As Figure 5 shows, the pore-pressure transducers are connected to a gutter that is incised along the circumference of the outer upper half of the shear box. The gutter is located 2 mm above the gap and is filled with a felt cloth filter sandwiched between two metal filters. It has an inside diameter of 12 cm and an outside diameter of 18 cm. The area of the shear surface is 141.4 cm^2, and the usual specimen height during shearing is about 6 cm. The shear displacement value is measured at the centre of the shear area. To prevent leakage of water from the gap between the upper and lower halves of the shear box, a rubber edge was glued onto the upper surface of the lower half of the shear box.

3.2 Pore-pressure behaviours

Specimens for the undrained ring shear test were formed by the air pluviation [Mulilis et al., 1977], since it provides the more uniform specimens [Gilbert & Marcuson 1988, Mooney et al. 1998]. The specimen was normally consolidated at total normal stress of 68.1 kPa and the initial shear stress was 41.5 kPa (which reproduced the 31-degree dipping slope) in considering the capacity of testing apparatus. The 15 cycles of sinusoidal shear stress was applied with the initial amplitude of 39.2 kPa, and then the amplitude was increased by 19.6 kPa for each cycle. The frequency of the cyclic shear stress was set at 1 Hz. After 15th cycle, the shear stress was kept constant at 41.5 kPa until the termination of the test.

Figure 6 presents the stress paths and the relationship between total normal stress, shear resistance, pore-pressure, and shear displacement versus elapsed time. During the test, it was controlled to produce a constant total normal stress, however, the fluctuation of 15 kPa at a maximum was observed because of the imperfectness of the control (Figure 6b). Shear resistance increased and decreased based on the cyclic shear stress loading, and at 7th cycle (4.72 mm shear displacement), it showed the peak value. After that it reduced its values not only during the cycling loading but also even after the cyclic loading. It reached constant values, that is steady sate [Poulos 1981] at about 2000 mm shear displacement. Because the input shear stress increased cycle by cycle, the difference between input values and the observed shear resistance became greater after 7th cycle. This difference in shear stress must accelerate the movement. It suggested that the cyclic shear stress loading built-up pore-pressure, and it suffered the strength loss that advanced the further shear displacement. Pore pressure, in general, increased within the whole processes of cyclic shear stress loading and the subsequent monotonic loading. But when looked more in detail, pore pressure decreased when the shear stress was applied in the forward direction and increased when the shear stress was applied in the backward (reverse) direction in view of each cycle (Figure 6b). It suggested that, since the specimen at the initial conditions was rather dense, the dilatancy took

place by the shear stress in the forward direction decreasing the pore pressure, and the shear stress in the backward direction produced negative dilatancy. This could be observed more clearly in Figure 6c that illustrates the pore pressure – shear displacement relationship. In each cycle, pore pressure is increased when shear displacement reduced its values due to shear stress in the backward direction, and pore pressure decreased when shear displacement progress due to shear stress in the forward direction. This process in each cycle gradually built-up pore pressure, it reached 45 kPa at the 15th cycle. When the cyclic loading finished, pore pressure was about 25 kPa, however it increased again by the monotonic shearing to reach 48 kPa at the steady state. The excess pore pressure ratio [Popescu, 1997] at the steady state was about 0.7, then quasi-liquefaction behaviours were observed. In the first stage of cyclic loading, because the shearing in the backward direction built-up the pore pressure, the cycling loading could be the vital trigger for the loss of shear resistance. The effective stress path exhibited the failure envelope line, suggesting the occurrence of sliding surface liquefaction behaviour (Figure 6a), and the effective angle of internal friction was about 36 degrees.

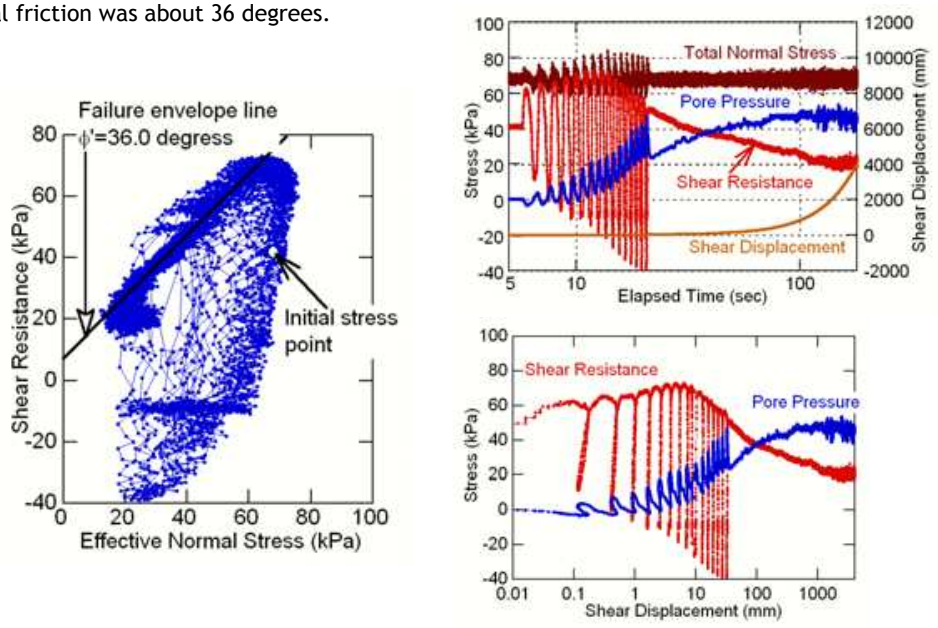

Figure 6: Results of the undrained ring shear test. a) the effective stress path, b) time series of total normal stress, pore pressure, shear resistance, and shear displacement, c) relationship of shear resistance and pore pressure to shear displacement

The relative changes in bulk permeability of the specimens before and after shearing are important to note. The bulk permeability of the specimen before shearing was $k' = 1.2\times10^{-5}$ m/s, whereas the bulk permeability after shearing was reduced to $k' = 3.3\times10^{-6}$ m/s. Movement of the sand particles is concentrated within the shear zone and this is associated with the particle breakages and the rearrangement of the particles. The permeability only within the shear zone must be smaller than the bulk permeability after shearing. This means that the less permeable structure was formed due to the shearing effect and it could prevent the dissipation of generated excessive pore pressure. The apparent friction angle at steady state was about 17 degrees. This 17 degrees is smaller than the travel angle (21 degrees), the low apparent friction angle associated with the high pore pressure ratio could explain the fluidised long run-out motion of the Haguro landslide.

4 NUMERICAL SIMULATION BY DISTINCT ELEMENT METHOD

The distinct element method [Cundall & Strack, 1979] was used to numerically reproduce in three dimensions the downslope run-out movement of the Haguro landslide. The calculation scheme is almost the same as Okada & Ochiai (2006). Although the sand particles have very complicated shapes, on the contrary, the shape of numerical elements, the balls in this study, are too simple and idealized. Because of this, the ball elements rotated too much in the past study (Okada & Ochiai, 2006). Iwashita et al. (1995) set up the rolling elastic spring and dashpot between disc or

ball elements in distinct element method for the rolling restraints, in which the geotechnical soil test conditions were reproduced. In this study, the rollings were simply not allowed during the movements.

Table 1: Input parameters for distinct element method

Parameter	Value
Normal elastic spring stiffness, K^n	$5.00\times10^{6.0}$ N/m
Tangential elastic spring stiffness, k^s	$1.25\times10^{6.0}$ N/m
Normal viscous damping coefficient, η^n	$2.27\times10^{5.0}$ Ns/m
Tangential viscous damping coefficient, η^s	$1.13\times10^{5.0}$ Ns/m
Coefficient of interparticle friction for initial packing	0.727
Coefficient of interparticle friction for flowing	0.310

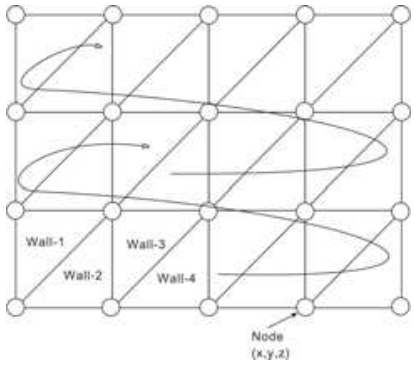

Figure 7: Scheme of wall elements formation using 10-m mesh digital terrain data

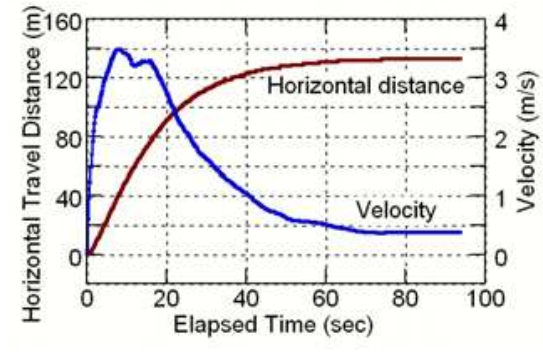

Figure 8: Horizontal travel distance and bulk velocity of granular mass flow

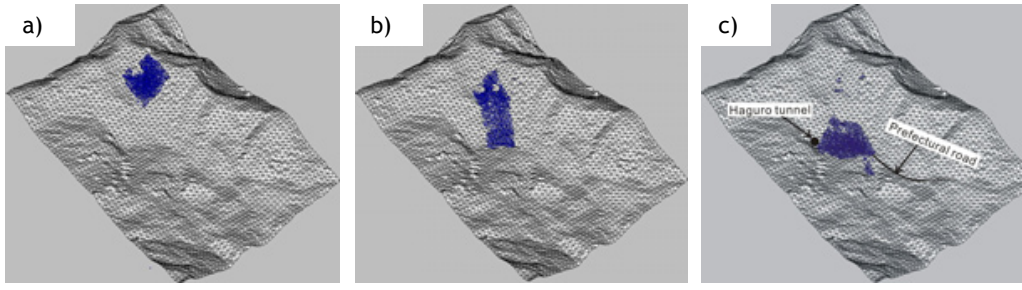

Figure 9: Downslope movement of granular mass flow. a) at initial packing, b) at a maximum bulk velocity, and c) at deposition.

Table 1 shows the input parameters used in the simulation. The digital terrain model around the Haguro landslide was produced using the data generated by laser profiling, in which wall elements designated by triangulated network were formed and combined as Figure 7 shows. The ball elements were produced in the zone of the depletion of the landslide with the interparticle friction angle of 36 degrees and with bonding forces between contacting balls being equal to gravity force, then the ball elements were deposited by self-weight under the gravity. When the average velocity of granular mass did not accelerate and reduced its values less than 0.1 m/s, it was assumed that the granular mass were packed at around the zone of depletion of the landslide. The radius of ball elements was randomly selected between 1.0 and 2.0 m. Totally 1964 ball elements were produced. Although the Haguro landslide took place due to the earthquake shakings, the deposited ball elements were mobilised downslope by simply reducing the interparticle friction to 17 degrees from a certain second, resembling the reduction of apparent friction angle in the undrained ring shear test. Figure 8 shows the horizontal travel distance at the gravity centre and the bulk velocity of the granular mass flow. The horizontal distance increased, then stayed almost constant from about 70 sec. The velocity showed the peak of 3.5 m/sec at about 7.5 sec and kept almost constant at

0.36m/sec from 70 sec. Figure 9 shows the process of movements of ball elements. The initially deposited ball elements travelled downslope with bulk velocity at 7.5 sec (Figure 9b), almost deposited on the prefectural road and blocked the Haguro tunnel (Figure 9c), in which it was observed that some ball elements moved further on the left hand bank. The calculated horizontal travel distance between the top of the headscarp before failure and the tip of the deposition was 267 m. Although the granular mass flow did not completely stop at the end of simulation, it reproduced well the horizontal travel distance and deposition observed in the field by the actual landslide, indicating it could be very effective method for the prediction of future landslide motion.

5 CONCLUSIONS

Pore pressure was mainly built-up by the cyclic shear stress loading in the undrained ring shear test. However, the pore pressure was further increased by the shear after the cyclic loading to reach steady state at which quasi-liquefaction was observed.

Since pore pressure decreased by the shearing in the forward direction and increased in the backward direction in each cycle of loading, it could be the cyclic loading that played a vital role for the fluidisation of the Haguro Landslide.

A simple and easy way of producing the digital terrain model by triangular wall elements for three-dimensional distinct element method was introduced and applied to the Haguro Landslide.

The ball elements produced for the zone of depletion of the landslide moved downslope to a similar deposit as observed for the Haguro landslide. This simulation method could be an effective tool for the prediction of travel area of the future landslides.

REFERENCES

Cundall, P.A., and Strack, O.D.L. (1979). *A discrete numerical model for granular assemblies*. Géotechnique. 29(1), 47-65

Gilbert, P.A., and Marcuson, W.F. (1988). *Density variation in specimens subjected to cyclic and monotonic loads*. Journal of Geotechnical Engineering Division, ASCE. 114(1), 1-20

Iwashita, K., Matsuura, K., and Oda, M. (1995). *Distinct element method with the effect of moment transfer at the contact points*. Proceedings of the Japan Society of Civil Engineers. 529(III-33), 145-154 (in Japanese)

Japan Meteorological Agency (2004). The Mid Niigata Prefecture Earthquake in 2004. http://www.jma.go.jp/JMA_HP/jma/press/0410/24a/name041024.pdf (in Japanese)

Mooney, M.A. Finno, R.J., and Viggiani, M.G. (1998). *A unique critical state for sand?* Journal of Geotechnical Engineering Division, ASCE. 112(10), 941-958

Mulilis, J.P., Seed, H.B., Chan, C.K., and Mitchell, J.K. (1977). *Effect of sample preparations on sand liquefaction*. Journal of Geotechnical Engineering Division, ASCE. 103(GT2), 91-108

Noguchi, S., Abdul, R.N., Zulkifli, Y., Tani, M., and Sammori, T. (1997). *Soil physical properties and preferential flow pathways in tropical rain forest, Bukit Tarek, Peninsula Malaysia*. Journal of Forest Research. 2, 125-132

Okada, Y., and Ochiai, H. (2006). *Simulating undrained triaxial compression behaviour by fluid-coupled distinct element method*. Proceedings of INTERPRAEVENT2006. 2, 447-453

Poulos, S.J. (1981). *The steady state deformation*. Journal of Geotechnical Engineering Division. 107(GT5), 553-562

Popescu, R., Prevost, J.H., and Deodatis, G. (1997). *Effects of spatial variability on soil liquefaction: some design recommendations*. Géotechnique. 47(5), 1019-1036